DOI: http://dx.doi.org/10.32571/ijct.1375421 **E-ISSN: 2602-277X**

International Journal of Chemistry and Technology

http://dergipark.org.tr/ijct

Research Article

Production and New Green Activation of Conductive 3D-Printed Cu/PLA Electrode: Its Performance in Hydrogen Evolution Reactions in Alkaline Media

Halil EKİCİ[1], Sevgi ATEŞ[2], Evrim BARAN AYDIN[2*]

[1]*Advanced Technology Application and Research Center (ATARC), Kilis 7 Aralık University Kilis, Türkiye*

[2]*Department of Chemistry, Faculty of Science, Advanced Technology Application and Research Center(ATARC), Kilis 7 Aralık University, Kilis, Türkiye*

Received: 13 October 2023; Revised: 29 December 2023; Accepted: 31 December 2023

*****Corresponding author e-mail: evrimbaran@kilis.edu.tr

Citation: Ekici, H.; Ateş, S.; Baran Aydın, E., *Int. J. Chem. Technol.* **2024**, 8(1), 32-44.

ABSTRACT

In this study, Cu-polylactic acid (PLA) composite filaments were produced with an extruder and three-dimensional (3D) Cu/PLA electrodes were 3D printed with Fused Deposition Modelling (FDM) method. To improve the electrochemical performance of the 3D-Cu/PLA electrode, a novel electrochemical activation method, which differentiates from complex activation methods in the literature, was applied in 1 M KOH solution without using any solvent. Field emission scanning electron microscopy (FE-SEM), Energy-Dispersive X-ray Spectroscopy (EDX), Fourier Transform Infrared Spectroscopy (FT-IR), and RAMAN techniques were used to characterize the 3D-Cu/PLA electrode before and after activation. The results showed that Cu particles were released after the degradation of PLA after activation. In addition, the thermal stability of the 3D electrode was demonstrated by the TGA technique. The performance of the 3D Cu/PLA electrode before and after activation in the hydrogen evolution reaction (HER) in 1M solution was measured using cyclic voltammetry (CV), electrochemical impedance spectroscopy (EIS), and cathodic polarization curves methods. The EIS results showed that the charge transfers resistance values of the 3D-Cu/PLA electrode in 1 M KOH decreased significantly after activation. Post-activation hydrogen content measurements of the 3D-Cu/PLA electrode after electrolysis at different potentials and energy efficiency tests at different current densities were also carried out. The results indicate that the electrocatalytic properties of 3D-Cu electrodes were improved for HER through the activation process.

Keywords: Cu-PLA, 3D electrode, FDM, hydrogen, Activation.

1. INTRODUCTION

Hydrogen is the most abundant element and accounted for approximately 90 % of all atoms in the universe.[1] It is a clean, versatile, and energy-dense fuel, which can be used to power a plethora of applications; including fuel cells, backup power systems, and industrial processes. Hydrogen has a calorific value of 120-142 MJ/kg, which is nearly three times as large as gasoline[2], which makes it a potentially important substitution for mainstream energy carriers. In addition, hydrogen has the potential to play a significant role in the transition to a cleaner, more sustainable energy future; since it only emits water and heat when combusted, can be obtained from a variety of resources including methane, biomass and natural gas. Especially, the use of renewable energy sources to produce hydrogen will facilitate the transition to a cleaner and zero-carbon future.[3]

There are different established methods in the literature and industry to produce hydrogen from different sources. These methods include gasification[4], steam methane reforming[5], pyrolysis[6], and water electrolysis.[7] However, the selected method for production should have a near-zero carbon footprint and low cost to make hydrogen a commercially viable alternative to fossil fuels. Among these methods, Steam methane reforming from natural gas has the lowest cost for hydrogen production with the drawback of a high carbon footprint. In contrast, the hydrogen cost of water electrolysis is the highest; but the carbon footprint of this method approaches zero when it is carried out with renewable energy.[8] The importance of electrolysis in hydrogen production lies in the fact that it can be used to produce hydrogen from renewable energy sources such as solar and wind power. When electricity generated from these sources is used to power the electrolysis process, the resulting hydrogen is considered to be "green" or "renewable" hydrogen, which is a clean alternative to fossil fuels.

DOI: http://dx.doi.org/10.32571/ijct.1375421 E-ISSN: 2602-277X

Therefore, reducing the hydrogen cost from water electrolysis is one of the most direct routes to elevate hydrogen as the main energy carrier in industrial and transport applications.

3D printing is a promising potential method for building electrodes for water splitting.[9-11] Fused deposition modeling (FDM) is the most commonly used, extrusion-based 3D printing method and proliferated to the point where it is used in custom home-built 3D printers. In this process, wire-shaped thermoplastic commonly referred to as filament, is fed through a hot heating block which leads to an extrusion nozzle. This extruder hot-end moves in vertical and horizontal directions based on the geometry to be printed, on a platform. Thus, the part is "printed" layer by layer on that building plate.[12]

3D printing has several advantages for producing complex electrode structures that can improve the efficiency and performance of water electrolysis systems. One advantage of 3D printing is that it allows for the production of customized and intricate electrode designs, which can optimize the surface area and distribution of active catalysts on the electrode surface.[13-15] This can increase the efficiency of water-splitting reactions and reduce the energy required for electrolysis. Another advantage of 3D printing is that it can facilitate the integration of multiple materials and components into a single electrode structure. For example, a 3D-printed electrode can incorporate different catalysts, conductive materials, and supports in a way that maximizes their effectiveness and improves the overall performance of the electrode. Additionally, 3D printing can enable the production of electrodes with unique geometries and architectures, such as porous or interconnected structures, that can enhance mass transport and improve the overall efficiency of water-splitting reactions.[16-18]

Graphene and carbon black are the fillers used for Polylactic Acid (PLA) thermoplastic filament material[16]. Foster et al. were the first group to utilize 3D printing to produce electrodes for energy storage. They found that graphene-PLA electrodes show promising catalytic activity toward hydrogen evolution reaction (HER).[19] However, these commercial graphene filaments only contain 8 wt % of graphene, therefore design and catalytic improvement are essential.[20] In 2018, Browne et al. applied an activation procedure that involves soaking in dimethylformamide (DMF) and applying constant potential for a certain period to their electrodes, which 3D printed with commercial PLA/Graphene filament. They reported that the solvent-electrochemical route significantly improves electrocatalytic activity.[21] Gusmão et al. spray-coated graphene/PLA electrodes with two-dimensional MoS_2 an obtained a 500 mV shift in the required overpotential at 10 mA cm^{-2} current density.[22] Browne and Pumera electrodeposited Nickel oxide to their DMF-treated graphene/PLA electrodes. They detected Ti, Fe, and Al impurities in their 3D printed electrodes through EDX analysis and argued that these impurities significantly increase catalytic activity.[23] Hughes et al. also reported that 2D-MoS_2, Pt and electro-conductive carbon increase the electrocatalytic activity of 3D-printed electrodes.[24] Several studies indicate that transition metal dichalcogenides increase the catalytic activity of 3D printed catalysts in both HER and oxygen evolution reactions (OER).

The catalyst plays a crucial role to lower the activation energy and increase the rate of the electrochemical reaction in the water-splitting process. Therefore, several catalyst materials were explored to make the process more efficient and cost-effective. For example, due to low cost and high conductivity, Copper is a highly preferable hydrogen evolution reaction (HER) electrode material. However, the introduction of catalytically active materials is crucial, since copper has low electrocatalytic activity.[25] Bui et al. 3D printed their electrodes from a conductive carbon-PLA filament and placed copper wires by stopping the print halfway. After the printing process, they electroplated the electrode with Nickel using Watt's nickel-plating solution. In their study, 50 mA cm^{-2} current density required the overpotentials of -0.6V and 0.8 V for HER and OER respectively.[11] Hüner et al. electrodeposited Nickel and copper on the commercial conductive filament and observed a 40.12 50 mA cm^{-2} current density at -1.4 V constant voltage.[26] Iffelsberger et al. used a commercial Copper/PLA filament to 3D print electrodes and doped different electrodes with Al_2O_3, TiO_2 and graphite through sinterization. They reported that Al_2O_3-doped photoelectrodes show the highest photo-electrochemical activity.[27]

To realize the industrialization of a process, scalability has the utmost importance. However, electrodeposition, solvent activation, and treatment with plating solutions and chemicals would be challenging and not cost-effective at the industrial scale. In addition, ready-to-use commercial conducting filaments are not sufficient for an effective water-splitting process. Instead, we propose a single-step production of a Cu/PLA composite catalyst with FDM 3D printing. Also, rather than a sophisticated activation process, we present a simple single-step activation. Therefore, we put forward a simple and scalable process to produce a catalyst for water splitting. In this study, the electrochemical activation process of the 3D Cu/PLA electrode produced by the FDM method from the prepared Cu/PLA filaments was carried out in 1M KOH solution. Characterization of the produced 3D Cu/PLA electrodes and Electrochemical measurements (EIS and TAFEL) in 1M KOH solution were taken before and after activation. The efficiencies of 3D Cu/PLA electrodes in hydrogen evolution reaction (HER) after the activation were demonstrated by

DOI: http://dx.doi.org/10.32571/ijct.1375421 E-ISSN: 2602-277X

measurements of hydrogen amount at different potentials and energy efficiency tests performed at different current densities. Also, the stability of the activated 3D electrode at low current density at different electrolysis times was also investigated.

2.EXPERIMENTAL

2.1. Materials

Copper powder (<63µm), chloroform (>99.95%), and potassium hydroxide (KOH) were purchased from Sigma Aldrich (St. Louis, Missouri, USA). PLA granules were supplied by Filameon Company (Kayseri, Turkiye). All chemicals were analytical grade and used without further purification or treatment.

2.2. Composite Filament Production

Initially, PLA granules (12 g, %30) were dissolved in chloroform (150 mL) at 55 °C in a closed container. Complete dissolution was achieved by stirring at regular intervals until a smooth homogenous solution is obtained. Following that, Copper powder (Cu percent by mass adjusted to 70 (28 g)) was subsequently introduced to the PLA solution and completely mixed via vigorous stirring. The mixture was dried in an oven until it takes a viscous dough form. The filament dough was cut into small pieces and dried under a vacuum until chloroform completely evaporates. Finally, the granular mixture was fed to a single screw Wellzoom extruder at (195°C, 1.75 mm) to produce composite filaments.

2.2.1. Electrode Production with 3D Printing

Electrode geometry was designed with open-source Free-CAD (version 0.20.2) software (Figure 1). Electrode Gcode generation was carried out with Repetier Host (version 2.3.1) software. Temperature settings were set to 215 °C and 55° C for the nozzle and print bed respectively. 3D printing was conducted with a custom-built Tronxy p802m printer. Nozzle diameter and layer thickness were selected as 1mm and 0.2 mm respectively. The surface area of the obtained 3D Cu/PLA electrode was calculated as 14.18 cm^2. Figure 1 shows electrode geometry designed with open-source FreeCAD, and images of Cu/PLA composite filament and 3D Cu/PLA electrode.

Figure 1. Electrode geometry designed with open-source FreeCAD (a), and images of Cu-PLA composite filament (b) and 3D Cu-PLA electrode (c).

2.2.2. Activation of the 3D-printed Electrode

The Cyclic voltammetry (CV) experiments were performed in the range of 0 V to -3 V at a scan rate of 100 mV/s for 4 cycles using a 3D electrode soaked in 1M KOH solution for one hour as the working electrode. In the second step, the process was repeated by attaching the electrode from the reverse side in order to activate the non-activated end of the 3D electrode.

2.2.3. Characterization of the 3D Cu/PLA

Surface features of 3D electrodes were analyzed by FEI Model Quanta 650 Field Emission-Scanning Electron Microscope (FE-SEM) at 10.00 kV EHT. Energy dispersive X-ray spectroscopy (EDX) integrated into the FE-SEM device was used to establish the percentage distribution of elements on the electrode surface. In order to determine the crystallography of activated 3D Cu/PLA using PANalytical EMPYREAN X-ray diffractometer (XRD), measurements were taken in the range of 2-theta values 20-85° under 45 kV and 40 mA Cu Kα radiation conditions. FT-IR spectra of the electrodes were obtained utilizing a JASCO FT/IR-6700 spectrometer in the wavelength range 4000-400 cm^{-1}. The thermal behaviour of the electrodes was investigated using a Shimadzu DTG-60H thermogravimetry/differential thermal analysis (TG/DTA) device at a heating rate of 10 °C/min under air atmosphere. Finally, Raman spectra (Renishaw in Via Qontor model) was acquired with a laser wavelength of 532 nm.

2.2.4. Electrochemical Measurements

The electrochemical properties of the 3D electrodes were investigated using electrochemical impedance spectroscopy (EIS), cyclic voltammetry (CV), and cathodic polarization curves recorded with an electrochemical analyzer (CHI604E) device with a three-electrode setup in 1M KOH solution before and after the activation. The reference electrode used was Ag/AgCl (3 M KCl), while a platinum plate with a surface area of 2 cm^2 was utilized as the counter electrode. EIS experiments were carried out at OCP, and

DOI: http://dx.doi.org/10.32571/ijct.1375421 E-ISSN: 2602-277X

the Zview software was employed to fit the impedance spectra results.

In order to calculate the overpotentials of the electrodes, the potentials were converted to reversible hydrogen electrode (RHE) utilizing equation (1).

$$E_{RHE} = E^0_{Ag/AgCl} + 0.059\ x\ pH + E^0_{Ag/AgCl} \quad (1)$$

$E^0_{Ag/AgCl}$ and $E_{Ag/AgCl}$ in Equation 1 are the standard and experimental potential values at room temperature, respectively. The current-potential measurements were obtained from open circuit potentials to -2 V with a scan rate of 5 mV s^{-1}. The CV analyses were conducted at a scan rate of 100 mV s^{-1} in the potential range of -2 to 0 V. Measurements of H_2 evolution of 3D Cu/PLA electrodes before and after activation were carried out under a voltage of -1.8, 2.0, and -2.2 V for 30 seconds. The H_2 gas formed during the 30 min treatment in 1 M KOH media was measured using an inverted burette. The amount of H_2 gas was expressed in mL. Energy consumption and efficiency tests of the electrodes for alkaline water electrolysis were carried out at current densities of 2.5, 5, and 10 mA cm^{-2} after 30 min electrolysis time in 1 M KOH media at 25 °C. In order to evaluate the stability of activated 3D Cu/PLA electrodes, a constant current of 5 mA cm^{-2} was applied to the electrode in 1 M KOH media at 25 °C for different times. After different electrolysis times (1 h, 2 h and 4 h), cathodic current-potential plots and EIS experiments (at open circuit potential) were performed utilizing CHI 604E A.C. electrochemical analyser.

3.RESULTS and DISCUSSION

Figure 2 demonstrated the activation CV measurements saved for 4 cycles of the 3D-Cu electrode in 1 M KOH media. Looking at the curves of the 3D-Cu electrode (Figure 2); It was observed that after -1.5 V in the first cycle, as seen from the increase in current intensity, the activation of the 3D electrode begins. After the third cycle, there is a sudden current increase from -0.6 V to -1.2 V. From -1.2 V to -1.4 V, the current decreases due to the conversion of copper to its oxide form. The increasing current values as a result of the cathodic cycle display that; As a result of the activation of the 3D-Cu electrode, PLA is broken down into sodium lactate and lactic acid as a result of alkaline hydrolysis of PLA (probability degradation reactions of PLA alkaline hydrolysis in Figure 3 [28] and the Cu particles embedded in PLA rise to the surface, increasing the conductivity of the 3D electrode. The FE-SEM results of the 3D-Cu electrode before and after the activation are presented in Figure 4 a and b, respectively. Before activation, the 3D-Cu electrode has indented layers on the surface of the electrode, in which PLA and Cu particles are embedded in each other, as shown in Figure 4 a.

After the activation process, the surface of the 3D-Cu electrode became much rougher. And on the surface of the 3D-Cu electrode, some degradation of polymeric chains occurred and Cu particles were exposed Figure 4 b. The EDX spectrums of the 3D-Cu electrode before and after the activation are given in Fig. 5 a-b.

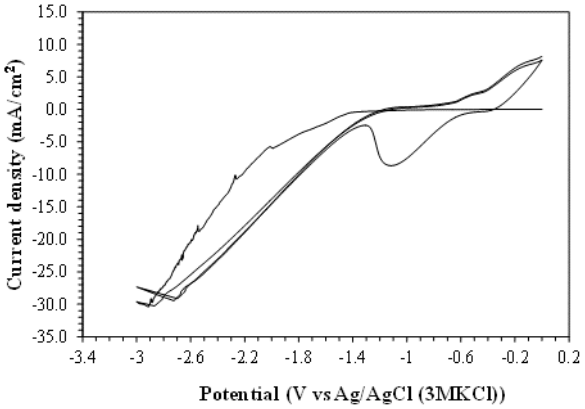

Figure 2. The cyclic voltammogram (CV) recorded for activation of the 3D-Cu/PLA electrode for 4 cycles at a scan rate of 0.1 V s^{-1} in 1 M KOH solution.

Accordingly, Cu contents before activation and after activation were determined as 47.06% and 49.04%, respectively. While the amounts of C and O before activation were 35.20% and 17.74%, respectively, the amounts of C and O after activation were found to be 34.79% and 16.17%. According to the EDX results, a partial increase was observed in the Cu content on the electrode surface as a result of the activation process, while a significant decrease was not observed in the amount of C and O. This shows that the degradation products (such as oligomers, lactic acid, and sodium lactate) formed after the activation process of polylactic acid are still trapped on the electrode surface. Also, with the degradation of the polymeric structure, the copper particles on the surface were exposed, causing a partial increase in the copper percentage. As a result, EDX spectra supported FE-SEM images.

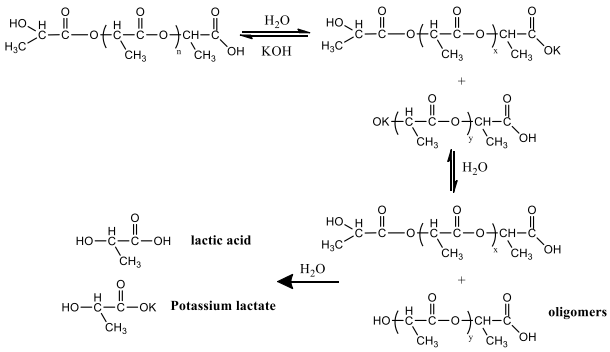

Figure 3. Probability degradation reactions of PLA alkaline hydrolysis.

DOI: http://dx.doi.org/10.32571/ijct.1375421 E-ISSN: 2602-277X

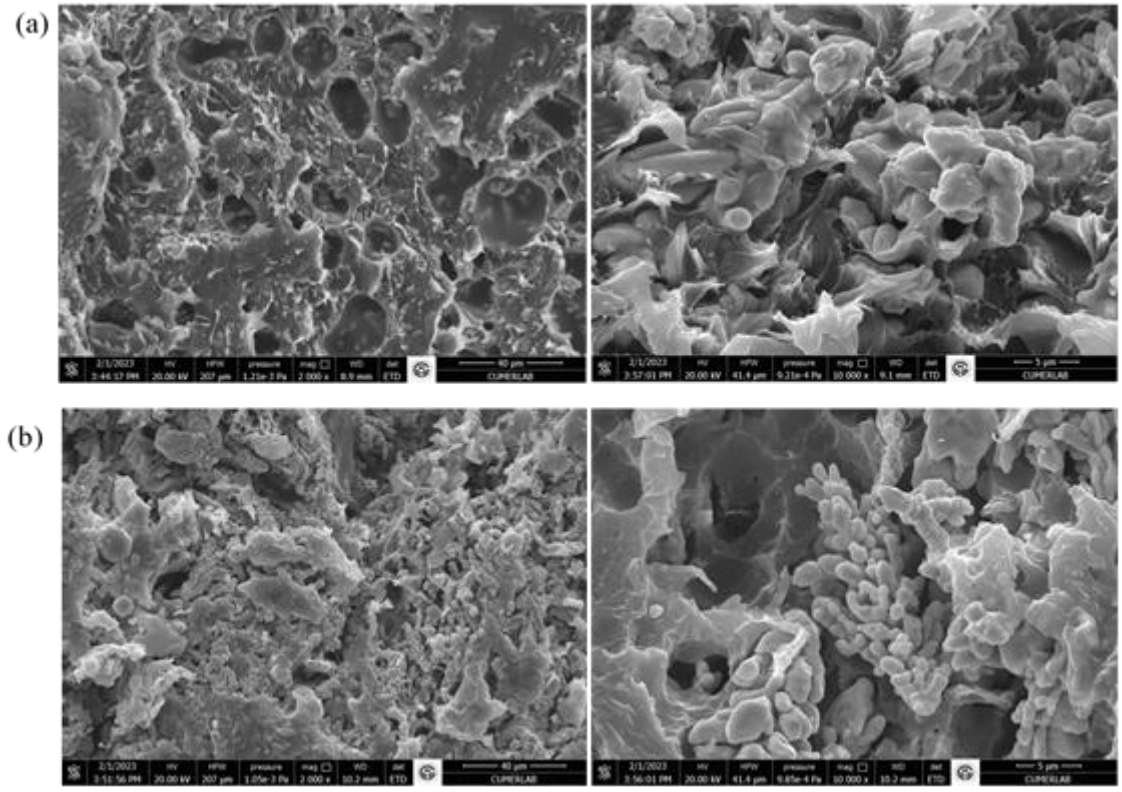

Figure 4. The FE-SEM images of the 3D-Cu/PLA electrode before (a) and after (b) the activation.

The XRD result recorded for the activated 3D Cu/PLA electrode is presented in Figure 6. The XRD peaks were indexed using JCPDS files (PDF card no. 04-0836) and the peaks at 42.88°, 49.95° and 73.75° corresponding to Miller indices (111), (200) and (220) are consistent with metallic copper and represent the face-centred cubic structure of copper. The XRD results showed that the 3D Cu/PLA electrode after activation has a pure copper phase without any impurity phase such as CuO, Cu_2O and $Cu(OH)_2$.

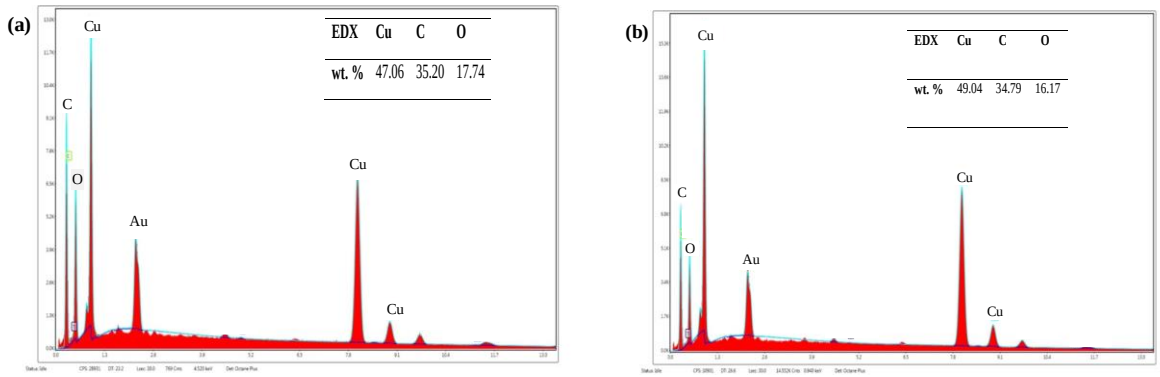

Figure 5. The EDX results of the 3D-Cu/PLA electrode before (a) and after (b) the activation.

Figure 7 displays FT-IR results of the obtained3D-Cu electrodes.It was observed that PLA peaks were dominant in the FT-IR spectra of 3D-Cu electrodes. The three bands at 1745, 1081 and 1180 cm^{-1} can be attributed to the characteristic strain frequencies for C=O, C–O, and C–O–C of PLA, respectively.[29, 30] In addition, peaks of two different bending frequencies were detected at 1380 cm^{-1} for $–CH_3$ asymmetric and 1555 cm^{-1} for $–CH_3$ symmetrical.In addition, it is clear from Figure 7 that these peak intensities of PLA reduced after activation of the 3D-Cu electrode.Thus, as a conclusion of activation in 1M KOH media, PLA degradation occurs in the 3D electrode and the existence of Cu particles is disclosed.

DOI: http://dx.doi.org/10.32571/ijct.1375421 **E-ISSN: 2602-277X**

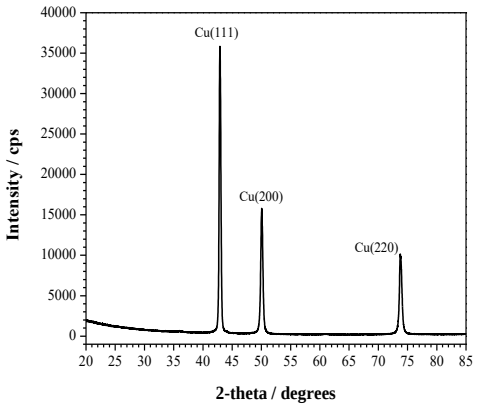

Figure 6. The XRD results of the 3D-Cu/PLA electrode after the activation.

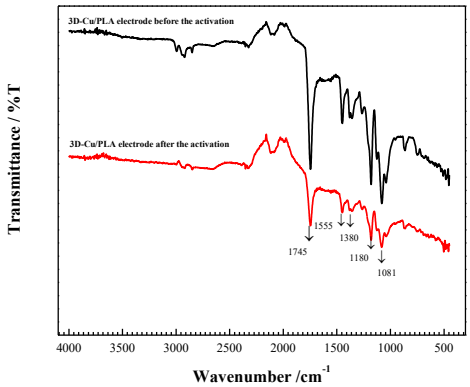

Figure 7. The FT-IR spectra of the 3D-Cu/PLA electrode before and after the activation.

Figure 8 illustrates Raman spectra for 3D-Cu electrodes before and after the activation. All the peaks demonstrated in Figure 8 are attributed to the chemistry of PLA macromolecular chains. These specific spectra of PLA; C-COO vibration at 869 cm^{-1}, CH_3 deformation vibrations at 1450 cm^{-1}, stretching vibrations of asymmetric C=O carboxylate groups at 1579 cm^{-1} and CH_3 at 2944 cm^{-1} show symmetrical and asymmetric stretching vibrations.[31] Moreover, it was observed that the broad flat peaks of PLA decreased significantly after the activation of the 3D-Cu electrode. Thus, the activation process of the 3D-Cu electrode in 1M KOH electrolyte significantly reduced the amount of PLA in the overall electrode.

The thermal decomposition of obtained 3D-Cu electrodes in the air atmosphere is presented in Figure 9. It shows a one-step decomposition (% weight loss) process. A weight loss of 30% between 350 and 450°C indicates that degradation of PLA has occurred.[32] The increase in mass between 400 and 500°C is related to the conversion of copper to its oxide form. In addition, while the mass loss of PLA was 30% before activation in the TGA curves of the 3D-Cu electrode, this value decreased to 27% after activation. This confirms that PLA decreases in the 3D electrode after activation.

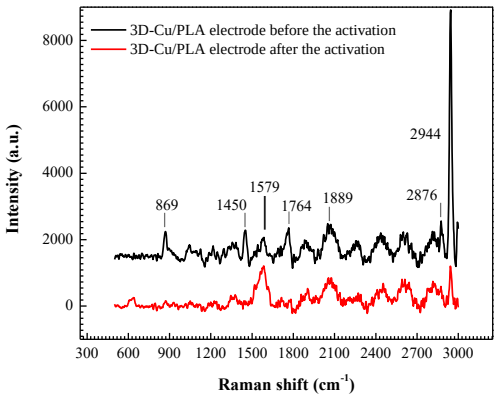

Figure 8. The Raman spectra of the 3D-Cu/PLA electrode before and after the activation.

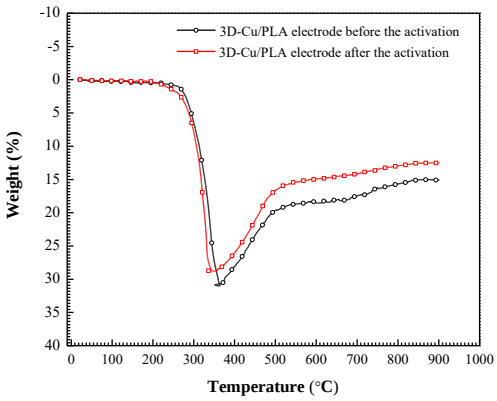

Figure 9. The TGA curves of the 3D-Cu/PLA electrode before and after the activation.

The OCP value as a function of time in 1 M KOH solution for the activated 3D-Cu electrode is given in Figure 10. It can be seen from Figure 10 that the activated 3D-Cu electrode shifts towards the more negative open circuit potential for up to about 600 seconds. This shows that: Activated 3D-Cu electrode shifting to negative potential begins to be active in the hydrogen formation reaction (HER). After about 1000 seconds, it shifts slightly to positive potentials and becomes stable after 3000 seconds. Electrochemical impedance spectroscopy (EIS) gives very significant information about the kinetic studies of electrochemical events. The EIS results recorded at open circuit potential for un-activated and activated 3D-Cu electrodes after 1 h immersion in 1 M KOH solution are presented as Nyquist and Bode plots in Figure 11 a-b. The Nyquist plots given in Figure 11 a consist of two parts, a semicircle, and a linear section. At high frequencies, the semicircle symbolize the electron transfer process, while the small linear part formed in the low-frequency region represents ion diffusion/transport in the electrolyte.[33]

DOI: http://dx.doi.org/10.32571/ijct.1375421 E-ISSN: 2602-277X

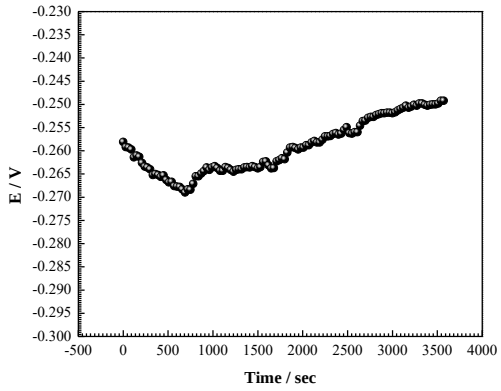

Figure 10. The open circuit potential-time curve of the 3D-Cu/PLA electrode in 1 M KOH solution at 25°C.

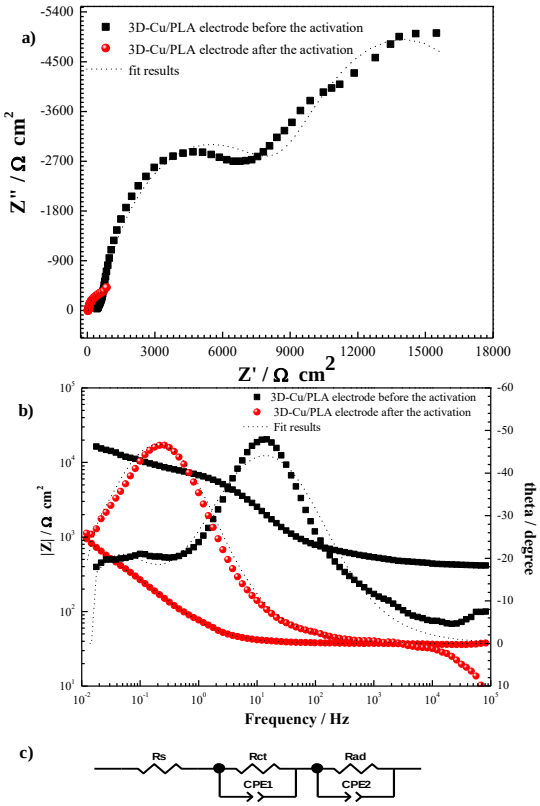

Figure 11. The Nyquist (a) and Bode (b) curves recorded at steady-state open circuit potential in 1 M KOH solution for 3D-Cu/PLA electrode before and after the activation, The used equivalent circuit model (c).

The obtained EIS plots were fitted utilizing the equivalent circuit models (Figure 11 c). The resulting fitting parameters are listed in Table 1. In the presented equivalent circuit model, two parallel combinations of R_{ct}/CPE_1, representing the charge transfer resistance and stationary phase element for the electrode reaction, and R_{ad}/CPE_2, representing the mass transfer resistance and stationary phase element for hydrogen adsorption, are used in series with a resistor (R_s) representing the solution resistance. In the equivalent circuit used, the stationary phase element was converted into a double-layer capacitance. The double-layer capacitance (C_{dl}) was calculated with the help of the parameters (Y, n) and resistance (R) values of the CPE using the following equation.[34]

$$C_{dl} = Y^{1/n} R^{(1-n)/n} \quad (2)$$

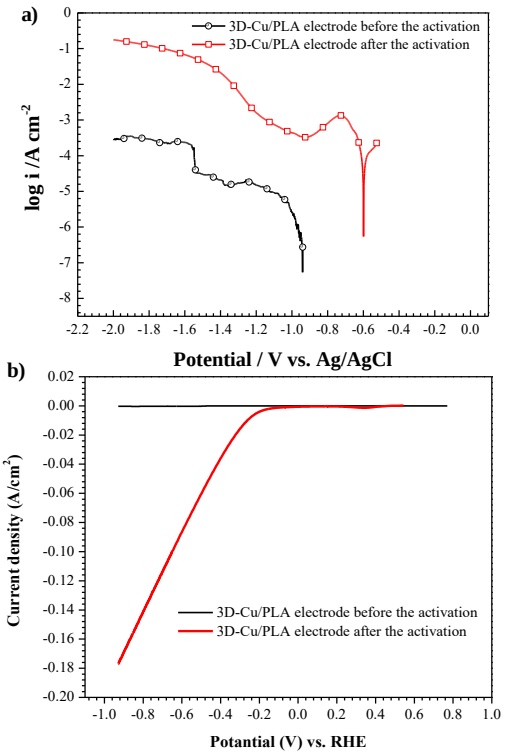

Figure 12. The cathodic polarization curves (a) and Current density-potential (vs. RHE) curves (b) of the 3D-Cu/PLA electrode before and after the activation obtained at steady-state open circuit potential in 1 M KOH solution at a scan rate of 0.001 V s^{-1}.

When the data obtained for the 3D-Cu electrode in Table 1 were examined, it was observed that the R_{ct} before activation was 10806 Ω cm^{-2}, while it decreased to 170 Ω cm^{-2} after activation. It was determined that while the R_{ad} value was 8707 Ω cm^{-2} before activation, it decreased to 735 Ωcm^{-2} after activation.The reduce in resistance values in this way can be attributed to the improvement of the electron transfer property of the 3D-Cu electrode by exposing the Cu particles embedded in PLA after activation. And thus, with the activation process, the H^+ adsorption in the active cathodic sites of the electrode increases, and the catalytic activity of HER is improved. Hüner et al. researched the hydrogen efficiency of the electrodes prepared by doping the surface of 3D electrodes synthesized with conductive graphene-based filament with different metal ratios of Nickel (Ni) and Platinum (Pt) in an alkaline medium.[35] They reported the charge transfer resistance (R_{ct}) values of $NiPt_1$, $NiPt_2$ and $NiPt_3$ coated 3D printed electrodes

DOI: http://dx.doi.org/10.32571/ijct.1375421 E-ISSN: 2602-277X

as 0.07502, 0.07561, and 0.07688 kΩ.cm^2 and hydrogen adsorption resistance (Rad) values as 0.6324, 0.5766 and 0.5704 kΩ.cm^2, respectively. Similarly, in another study, Hüner et al. deposited Ni and Cu metals at different volume ratios on the surface of 3D electrodes made with conductive PLA filament at 10 V to obtain high kinetic activity.[26] They reported the Rct values of these 3D electrodes (NixCux, NixCu2x, and NixCu3x) as 39.667, 0.262, 0.193, and 0.187 kΩ and Rad values as 0, 1.52, 1.13, and 0.62 kΩ, respectively, obtained from Nyquist curves in alkaline medium.Comparing the studies summarised above with the presented work, it is seen that the activated three-dimensional conductive Cu/PLA composite electrodes exhibit resistance values low enough to compete with 3D electrodes doped with elements such as nickel and platinum, which are known to be highly active in HER. In addition, with this method, it is possible to produce HER-active electrodes at more affordable prices with fewer procedures.

Table 1. The parameters obtained from fitting the EIS data in 1 M KOH test solution at open circuit potential.

3D Cu/PLA Electrodes	R_{ct} (Ω cm^2)	CPE_1 (S^n Ω^{-1}cm^{-2})	n_1 (Ω cm^2)	Cdl_1 (□F cm^{-2})	R_{ad} (Ω cm^2)	CPE_2 (S^n Ω^{-1}cm^{-2})	n_2 (Ω cm^2)	Cdl_2 (□F cm^{-2})
Before Activation	10806	4x10^{-4}	0.88	1940	8707	2x10^{-5}	0.71	1170
After Activation	170	1x10^{-3}	0.64	26200	735	7x10^{-3}	0.86	25100

In addition, it was determined from Table 1 that there was a significant increase in the C_{dl1} and C_{dl2} values of the 3D-Cu electrode after activation. This is attributed to the trap states where the injected electrons are widely dispersed after activation, with the Cu particles in the Cu-PLA composite being exposed from the surface. Thus, the increase of copper on the electrode surface, which is released from the Composite after activation, increases the capacitance of the space charge layer by providing higher electron donor states. Other than that, the single peak in the Bode curve shown in Figure 11 b ascribed to relaxation,that is associated with the charge transfer phenomenon.[36] In addition, the optimum oscillation frequency of the impedance semicircle of the 3D-Cu electrode after activation was found to be lower compared to pre-activation; This indicates that the post-activation 3D-Cu electrode has a higher electron recombination lifetime.[37]

Potentiodynamic polarization experiments was performed for researching the electrocatalytic activity of the obtained 3D-Cu electrodes toward HER and the results are presented in Figure 12 a. The cathodic Tafel slopes (βc), Open Circuit Potential ($\mathbf{E_{ocp}}$), and exchange current densities (J_o) were determined from these curves and listed in Table 2. It is clear from Figure 12 a and the values in Table 2 that the current density of the activated 3D-Cu electrode significantly increased compared to the un-activated 3D-Cu electrode. This increase shows that as a result of activation in 1 M KOH media, the appearance of Cu particles providing conductivity in the structure of the 3D-Cu electrode, the pores in the electrode structure clogged during hydrogen formation are opened and the electrocatalytic active surface area increases. Volmer, Heyrovsky, and Tafel deterministic rate steps corresponding to Tafel slopes of -120, -40 and -30 mV dec^{-1}, respectively, are widely used for kinetic models of HER. The Tafel slopes for un-activated and activated 3D-Cu electrodes were found as -75 and -120 mV dec^{-1}, respectively. As investigated the cathodic Tafel slopes given in Table 2, indicates that the charge transfer (Volmer) reaction is the rate-determining step for HER, and HER is limited by the hydrogen adsorption reaction to form M-H_{ads} intermediates[38]. As shown in Figure 12 b, the overpotential values for the HER of the 3D Cu/PLA electrode after activation at 10 mA/cm^2 were determined as -0.262 V (vs RHE). The results displayed that there was a significant decrease in the overpotential of the 3D Cu/PLA electrode after activation compared to before activation.

Table 2. The parameters obtained from Cathodic polarization measurement results.

3D-Cu/PLA Electrodes	E_{ocp} (V)	J_o (mA cm^{-2})	βc (mV dec^{-1})
Before Activation	-0.941	4.36x10^{-4}	75
After Activation	-0.599	0.173	120

Figure 13 showed that the CV measurements saved for 4 cycles of the 3D-Cu electrodes in 1 M KOH solution before and after the activation. When the CV measurements of the 3D electrode before activation are examined, it is seen that there is a peak belonging to the oxidation of copper (Cu_2O and $Cu(OH)_4^{-2}$) with a very low current density value of around -0.4 V in the anodic direction in the first and second cycles in accordance with the literature[39] and in the 4th cycle, it is seen that Cu_2O and $Cu(OH)_4^{-2}$ species are reduced to Cu with very low current density values at -0.9 V. Before activation, as can be seen from the CV, the current increases as you go towards the cathodic direction at -1.8 V in the 4th cycle and the current density values were determined as -0.15 mA/cm^2, -0.21 mA/cm^2 and -0.27 mA/cm^2 at -1.8 V, 2 V, and -2.2 V, respectively. After activation, the formation peaks of Cu_2O and $Cu(OH)_4^{-2}$ species were observed at about -0.5 V in the anodic direction due to the copper particles released by the breakdown of PLA molecules, while the reduction peaks of Cu_2O and $Cu(OH)_4^{-2}$ species to Cu at approximately -1 V and -1.3 V in the cathodic direction are seen. After activation, it is seen that the current density values are -8.67 mA/cm^2, -12.44 mA/cm^2 and -15.57 mA/cm^2 at -1.8 V, 2 V, and -2.2 V respectively in the fourth cycle. The CV results show that as a result of

DOI: http://dx.doi.org/10.32571/ijct.1375421 E-ISSN: 2602-277X

the activation process applied, the copper active centers on the surface of the 3D electrodes come to the surface and come into contact with the solution, resulting in an increase in current density by approximately 57 times.

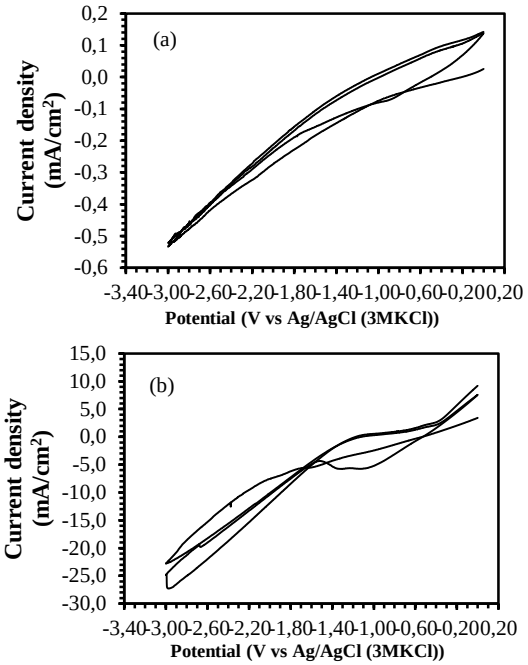

Figure 13. The cyclic voltammograms of the unactivated (a) and activated 3D-Cu/PLA electrode (b) recorded for 4 cycles at a scan rate of 0.1 V s^{-1} in 1 M KOH solution.

The amount of hydrogen gas measured at different potentials was determined as 10 mL at -1.8 V, 20 mL at -2 V, and 32 mL at -2.2 V. As can be seen from Figure 14 b-c, the total amount of charge passing through the circuit for -1.8 V, -2 V, and 2.2 V during hydrogen evolution before activation was -5.39x10^{-7}C, -2.53x10^{-1} C and -2.59x10^{-1} C, respectively, and after activation -8.97x10^{1}C, -1.53x10^{2}C and -2.30x10^{2} C after activation, respectively. As can be seen from the results, the hydrogen volume is zero at all potentials before activation, and as a result of activation, the electrode is activated due to the Cu particles released as a result of the breakdown of PLA on the surface, and the total charge and hydrogen gas volume passing through the circuit increases in proportion to the potential increase.

The energy consumption (Q) and energy efficiency (η_{HHV}) for HER on activated 3D-Cu electrodes at 2, 5, and 10 mA cm^{-2} current densities at 25 °C were determined using the following equations:[34, 40]

$$Q = I.U.t \quad (3)$$

$$\eta_{HHV} = \frac{283.3kJ/mol}{U.I.t} \quad (4)$$

Where U is the cell voltage (V) and as well as A is the applied current. t is a time of evolution of1 mol of hydrogen in seconds.

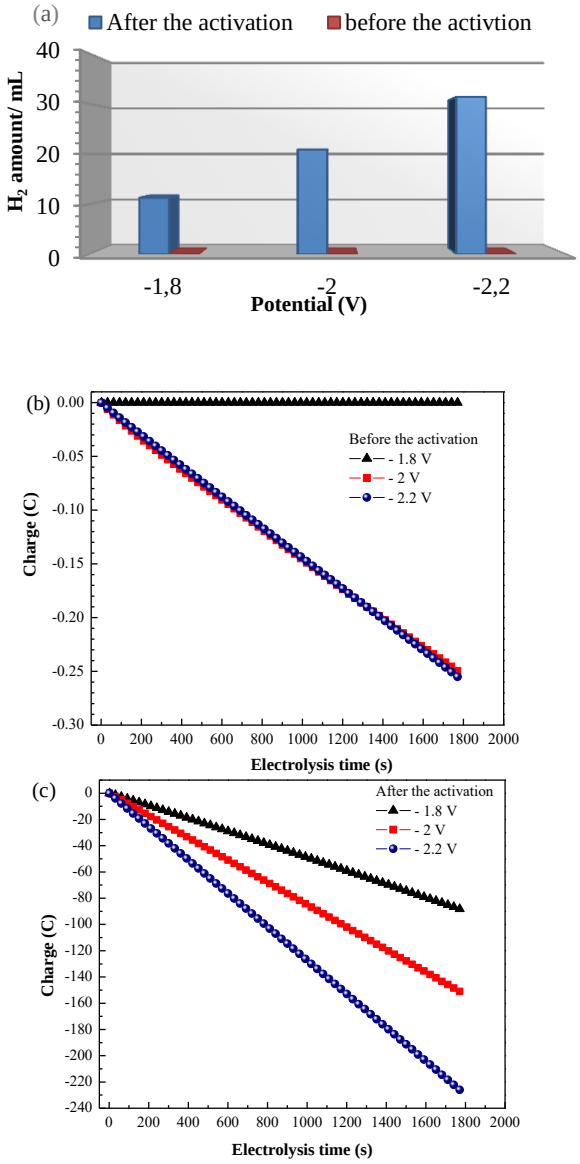

Figure 14. Hydrogen evolution amounts obtained on the 3D-Cu/PLA electrodes before and after the activation in 1 M KOH solution at different potentials (a) and Charge-electrolysis time curves of the unactivated (b) and activated 3D-Cu/PLA electrode obtained in 1 M KOH solution.

The obtained results are given in Figure 15. Energy consumption values increase considerably with increasing current densities as seen in Figure 15. Energy consumption values obtained for the activated 3D-Cu electrode; It was found to be 285.92 kJ mol^{-1} for 2 mA cm^{-2} current density, 301 kJ mol^{-1} for 5 mA cm^{-2} current density and 416 kJ mol^{-1} for 10 mA cm^{-2} current density. On the other hand, it was observed from Figure 15 b that the energy efficiency values decreased with increasing current density. Energy efficiency values of the activated 3D-Cu electrode; It was determined as 99% for 2 mA cm^{-2} current density, 93% for 5 mA cm^{-2} current density, and 67% for 10 mA cm^{-2} current density.

DOI: http://dx.doi.org/10.32571/ijct.1375421 E-ISSN: 2602-277X

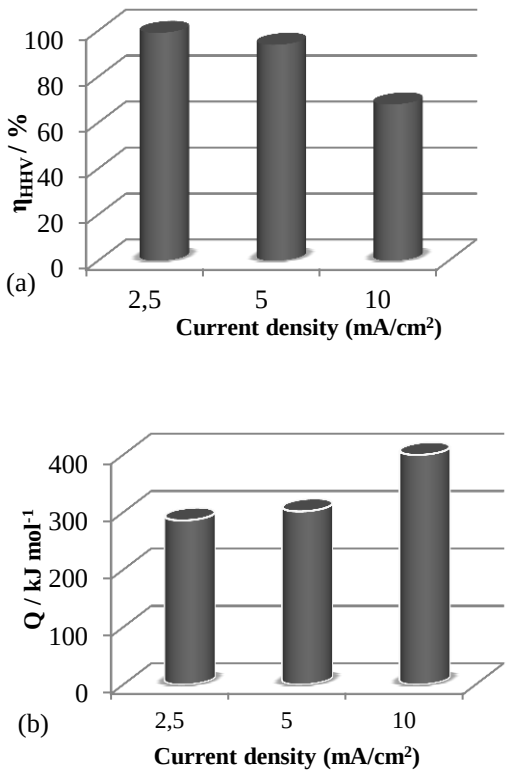

Figure 15. Energy consumption (a) and efficiency (b) on the activated 3D-Cu/PLA electrode in 1 M KOH solution at different current densities.

The Nyquist curves recorded after certain times (1 h, 2 h and 4 h) after applying a current density of 5 mA/cm^2 in 1M KOH solution to the activated 3D Cu/PLA electrode are presented in Figure 16 a. The obtained Nyquist curves were fitted utilizing the equivalent circuit given in Figure 11 c. R_{ct} values calculated after 1 h, 2 h and 4 h were 49.5, 60.29 and 27.32 Ω cm^{-2}and R_{ad} values were 1462, 1974 and 1196Ω cm^{-2}, respectively. After 4 hours of electrolysis time, the slight decrease in R_{ad} value indicates the activation of the electrode by electrolysis and the acceleration of electron transfer in the catalytic regions of the electrode after 4 hours of electrolysis. However, the disintegration of the Cu electrode due to the degradation of PLA molecules in the 3D Cu/PLA electrode after 4 h of electrolysis in alkaline medium showed that the 3D electrode was not stable even at low current densities.

The cathodic current-potential curves of the electrodes after 1, 2 and 4 h electrolysis is given in Figure 16 b. The cathodic Tafel slopes (β_c) of the activated 3D Cu/PLA electrode were determined from the linear part of the cathodic current-potential curves and the β_c values were determined as -114.7 mV dec^{-1} 250.3 mV dec^{-1} and 149.9 mV dec^{-1} after 1 h, 2 h and 4 h electrolysis, respectively.

As can be seen from the calculated values, it is seen that the rate determining step is the Volmer step. The lack of large changes in Tafel slopes during the 4 h electrolysis time shows that the HER mechanism does not change during the 4 h electrolysis time and the electrochemical stability of the activated 3D electrode for HER is limited to 4 h. FE-SEM and EDX images of the activated 3D Cu/PLA electrode after electrolysis at a current density of 5 mA/cm^2 for 4 hours are presented in Figure 17. As can be seen from the figure, it is clearly seen that the PLA molecules, which act as binders in the electrode, disintegrate and Cu particles are completely exposed.

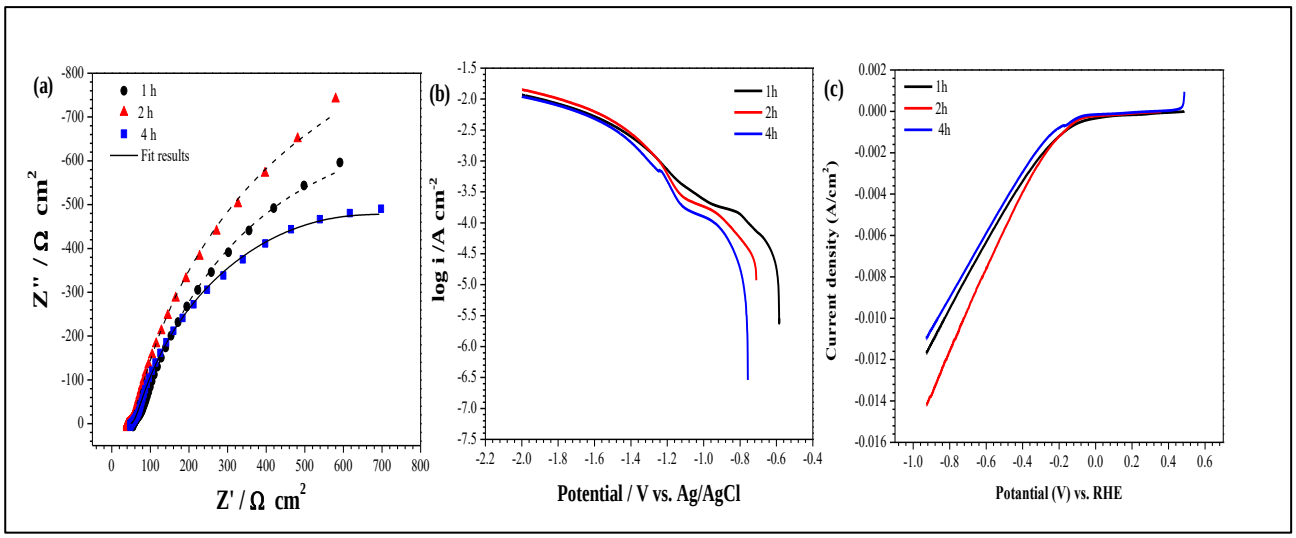

Figure 16. The Nyquist (a), the cathodic polarization (b) and current density-potential (vs. RHE) curves (c) recorded for the activated 3D-Cu/PLA electrode after the different electrolysis time.

DOI: http://dx.doi.org/10.32571/ijct.1375421 E-ISSN: 2602-277X

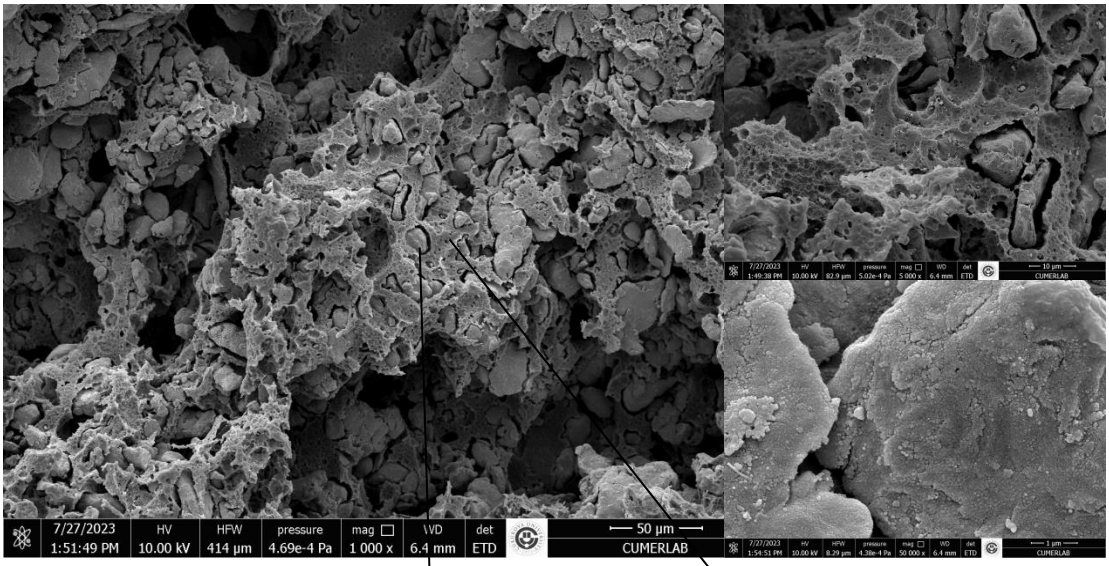

Element	Weight %	Atomic %	Net Int.
Cu	100	100	648.8

Element	Weight %	Atomic %	Net Int.
C	60.66	76.88	941.72
O	19.24	18.3	210.76
Cu	20.1	4.82	82.57

Figure 17. The FE-SEM images and EDX results of the activated 3D-Cu/PLA electrode after the electrolysis time of 4 h.

4.CONCLUSION

As a result of this study, Cu/PLA composite filaments were produced and 3D-Cu printed electrodes were successfully fabricated by the Fused Deposition Modeling (FDM) method. Moreover, a new activation method was applied in 1 M KOH solution, different from the literature, in order to improve the conductivity of the 3D-Cu electrode. The morphology and composition of the electrodes were determined by FE-SEM and EDX techniques. The FE-SEM results showed that while PLA and Cu particles were embedded in each other on the surface of the 3D-Cu electrode before activation, after the activation process, PLA decomposed and Cu particles were exposed. In addition, after activation of the 3D-Cu electrode, As a result of the disintegration of PLA, copper particles on the surface were exposed, causing a partial increase in the percentage of copper on the surface, and FE-SEM images supported the EDX results. In addition, FT-IR and Raman analyses of activated and non-activated 3D-Cu electrodes were performed and the effect of the activation process on the changes in the structure was investigated. As a result of the TGA measurements of the obtained 3D-Cu electrodes in the air atmosphere, a mass loss due to the degradation of PLA was observed. While this mass loss was 30% before activation, it decreased to 27% after activation. The EIS results indicated that charge transfer resistance value was 10806 Ω cm^{-2} before activation, it decreased to 170 Ωcm^{-2} after activation. The cathodic polarization results show that the Volmer mechanism is the rate-determining step for HER. In addition, it was determined that the current density of the activated 3D-Cu electrodes increased significantly compared to the inactive 3D-Cu electrode. Furthermore, the energy consumptions of the activated 3D-Cu electrodes were increased with current densities. The experimental results obtained showed that the activated 3D-Cu electrodes improved the electrocatalyst properties for HER through the activation process. The stability test of the activated 3D Cu/PLA electrode at low current density showed that the stability time of the electrode was 4 hours due to the disintegration of the PLA molecule in alkaline medium.

DOI: http://dx.doi.org/10.32571/ijct.1375421 **E-ISSN: 2602-277X**

ACKNOWLEDGEMENTS

The authors are thankful to the Kilis 7 Aralık University research fund (Project number: 22/MAP/004) for their financial support.

Conflict of Interest

Authors declare that there is no a conflict of interest with any person, institute, company, etc.

REFERENCES

1. Grochala, W. First there was hydrogen. *Nat. Chem.* **2015**, *7* (3), 264-264.
2. McCay, M.; Shafiee, S.; Letcher, T. Future Energy. **2020**.
3. Nikolaidis, P.; Poullikkas, A. A comparative overview of hydrogen production processes. *Renew. Sust. Energ Rev.* **2017**, *67*, 597-611.
4. Porshnov, D. Evolution of pyrolysis and gasification as waste to energy tools for low carbon economy. *Wires. Energy Environ.* **2022**, *11* (1), e421.
5. Saeidi, S.; Sápi, A.; Khoja, A. H.; Najari, S.; Ayesha, M.; Kónya, Z.; Asare-Bediako, B. B.; Tatarczuk, A.; Hessel, V.; Keil, F. J. Evolution paths from gray to turquoise hydrogen via catalytic steam methane reforming: Current challenges and future developments. *Renew. Sust. Energ Rev.* **2023**, *183*, 113392.
6. Chen, C.; Teng, Z.; Yasugi, M.; Yang, H.; Cao, Y.; Yu, L.; Ohno, T. A homogeneous copper bismuth sulfide photocathode prepared by spray pyrolysis deposition for efficient photoelectrochemical hydrogen generation. *Mater. Lett.* **2022**, *325*, 132801.
7. Da Silva Veras, T.; Mozer, T. S.; da Silva César, A. Hydrogen: trends, production and characterization of the main process worldwide. *Int. J. Hydrogen Energ.* **2017**, *42* (4), 2018-2033.
8. Ji, M.; Wang, J. Review and comparison of various hydrogen production methods based on costs and life cycle impact assessment indicators. *Int. J. Hydrogen Energ.* **2021**, *46* (78), 38612-38635.
9. Guvendiren, M.; Molde, J.; Soares, R. M.; Kohn, J. Designing biomaterials for 3D printing. *ACS Biomater. Sci. Eng.* **2016**, *2* (10), 1679-1693.
10. Gross, B.; Lockwood, S. Y.; Spence, D. M. Recent advances in analytical chemistry by 3D printing. *Anal. Chem.* **2017**, *89* (1), 57-70.
11. Bui, J. C.; Davis, J. T.; Esposito, D. V. 3D-Printed electrodes for membraneless water electrolysis. *Sustain. Energ. Fuels* **2020**, *4* (1), 213-225.
12. Li, N.; Tong, K.; Yang, L.; Du, X. Review of 3D printing in photocatalytic substrates and catalysts. *Mater. Today Energy* **2022**, 101100.
13. Ngo, T. D.; Kashani, A.; Imbalzano, G.; Nguyen, K. T.; Hui, D. Additive manufacturing (3D printing): A review of materials, methods, applications and challenges. *Compos. B Eng.* **2018**, *143*, 172-196.
14. Baş, F.; Kaya, M. F. 3D printed anode electrodes for microbial electrolysis cells. *Fuel* **2022**, *317*, 123560.
15. Rohaizad, N.; Mayorga-Martinez, C. C.; Novotný, F.; Webster, R. D.; Pumera, M. 3D-printed Ag/AgCl pseudo-reference electrodes. *Electrochem. Commun.* **2019**, *103*, 104-108.
16. Zhang, X.; Guo, K.; Shen, D.; Feng, H.; Wang, M.; Zhou, Y.; Jia, Y.; Liang, Y.; Zhou, M. Carbon black as an alternative cathode material for electrical energy recovery and transfer in a microbial battery. *Sci. Rep.* **2017**, *7* (1), 1-10.
17. Gong, Y.; Li, D.; Fu, Q.; Pan, C. Influence of graphene microstructures on electrochemical performance for supercapacitors. *Prog. Nat. Sci.: Mater. Int.* **2015**, *25* (5), 379-385.
18. Browne, M. P.; Urbanova, V.; Plutnar, J.; Novotný, F.; Pumera, M. Inherent impurities in 3D-printed electrodes are responsible for catalysis towards water splitting. *J. Mater. Chem. A* **2020**, *8* (3), 1120-1126.
19. Foster, C. W.; Down, M. P.; Zhang, Y.; Ji, X.; Rowley-Neale, S. J.; Smith, G. C.; Kelly, P. J.; Banks, C. E. 3D printed graphene based energy storage devices. *Sci. Rep.* **2017**, *7* (1), 42233.
20. Browne, M. P.; Redondo, E.; Pumera, M. 3D printing for electrochemical energy applications. *Chem. Rev.* **2020**, *120* (5), 2783-2810.
21. Browne, M.; Novotný, F. Z. k. Sofer and M. Pumera. *ACS Appl. Mater. Interfaces* **2018**, *10*, 40294-40301.
22. Gusmão, R.; Sofer, Z.; Marvan, P.; Pumera, M. MoS 2 versatile spray-coating of 3D electrodes for the hydrogen evolution reaction. *Nanoscale* **2019**, *11* (20), 9888-9895.
23. Browne, M. P.; Pumera, M. Impurities in graphene/PLA 3D-printing filaments dramatically

DOI: http://dx.doi.org/10.32571/ijct.1375421 **E-ISSN: 2602-277X**

influence the electrochemical properties of the devices. *Chem. Commun.* **2019**, *55* (58), 8374-8377.

24. Hughes, J. P.; dos Santos, P. L.; Down, M. P.; Foster, C. W.; Bonacin, J. A.; Keefe, E. M.; Rowley-Neale, S. J.; Banks, C. E. Single step additive manufacturing (3D printing) of electrocatalytic anodes and cathodes for efficient water splitting. *Sustain. Energy Fuels* **2020**, *4* (1), 302-311.

25. Yang, W.; Chen, S. Recent progress in electrode fabrication for electrocatalytic hydrogen evolution reaction: A mini review. *J. Chem. Eng.* **2020**, *393*, 124726.

26. Huener, B.; Demir, N.; Kaya, M. F. Electrodeposition of NiCu bimetal on 3D printed electrodes for hydrogen evolution reactions in alkaline media. *Int. J. Hydrogen Energ.* **2022**, *47* (24), 12136-12146.

27. Iffelsberger, C.; Rojas, D.; Pumera, M. Photo-Responsive Doped 3D-Printed Copper Electrodes for Water Splitting: Refractory One-Pot Doping Dramatically Enhances the Performance. *J. Phys. Chem. C* **2022**, *126* (21), 9016-9026.

28. Siddiqui, M. N.; Kolokotsiou, L.; Vouvoudi, E.; Redhwi, H. H.; Al-Arfaj, A. A.; Achilias, D. S. Depolymerization of PLA by phase transfer catalysed alkaline hydrolysis in a microwave reactor. *J. Polym. Environ.* **2020**, *28*, 1664-1672.

29. Chieng, B. W.; Ibrahim, N. A.; Wan Yunus, W. M. Z.; Hussein, M. Z. Poly (lactic acid)/poly (ethylene glycol) polymer nanocomposites: Effects of graphene nanoplatelets. *Polymers* **2013**, 6 (1), 93-104.

30. Pop, M. A.; Croitoru, C.; Bedő, T.; Geamăn, V.; Radomir, I.; Cos, n., ă, Mihaela; Zaharia, S. M.; Chicos, L. A.; Milos, a., Ioan. Structural changes during 3D printing of bioderived and synthetic thermoplastic materials. *J. Appl. Polym. Sci.* **2019**, 136 (17), 47382.

31. Vidakis, N.; Petousis, M.; Velidakis, E.; Mountakis, N.; Tzounis, L.; Liebscher, M.; Grammatikos, S. A. Enhanced mechanical, thermal and antimicrobial properties of additively manufactured polylactic acid with optimized nano silica content. *Nanomaterials* **2021**, 11 (4), 1012.

32. Vu, M. C.; Jeong, T. H.; Kim, J. B.; Choi, W. K.; Kim, D. H.; Kim, S. R. 3D printing of copper particles and poly (methyl methacrylate) beads containing poly (lactic acid) composites for enhancing thermomechanical properties. *J. Appl. Polym. Sci.* **2021**, *138* (5), 49776.

33. Pusomjit, P.; Teengam, P.; Thepsuparungsikul, N.; Sanongkiet, S.; Chailapakul, O. Impedimetric determination of cortisol using screen-printed electrode with aptamer-modified magnetic beads. *Mikrochim. Acta* **2021**, *188*, 1-8.

34. Herraiz-Cardona, I.; Ortega, E.; Vázquez-Gómez, L.; Pérez-Herranz, V. Electrochemical characterization of a NiCo/Zn cathode for hydrogen generation. *Int. J. Hydrogen Energ.* **2011**, *36* (18), 11578-11587.

35. Hüner, B.; Demir, N.; Kaya, M. F. Ni-Pt coating on graphene based 3D printed electrodes for hydrogen evolution reactions in alkaline media. *Fuel* **2023**, *331*, 125971.

36. QayoomáMugheri, A.; LiaquatáBhatti, A.; NaeemáMemon, N.; IshaqueáAbro, M.; AhmedáShah, A.; AliáHullio, A.; HussainálbupoTo, Z. Efficient tri-metallic oxides NiCo 2 O 4/CuO for the oxygen evolution reaction. *RSC Adv.* **2019**, *9* (72), 42387-42394.

37. Song, Q.; Li, J.; Wang, L.; Qin, Y.; Pang, L.; Liu, H. Stable single-atom cobalt as a strong coupling bridge to promote electron transfer and separation in photoelectrocatalysis. *J. Catal.* **2019**, *370*, 176-185.

38. Bao, F.; Kemppainen, E.; Dorbandt, I.; Bors, R.; Xi, F.; Schlatmann, R.; van de Krol, R.; Calnan, S. Understanding the Hydrogen Evolution Reaction Kinetics of Electrodeposited Nickel-Molybdenum in Acidic, Near-Neutral, and Alkaline Conditions. *ChemElectroChem* **2021**, 8 (1), 195-208.

39. Giri, S. D.; Sarkar, A. Electrochemical study of bulk and monolayer copper in alkaline solution. *J Electrochem. Soc.* **2016**, 163 (3), H252.

40. Nikolic, V. M.; Tasic, G. S.; Maksic, A. D.; Saponjic, D. P.; Miulovic, S. M.; Kaninski, M. P. M. Raising efficiency of hydrogen generation from alkaline water electrolysis–Energy saving. *Int. J. Hydrogen Energ.* **2010**, 35 (22), 12369-12373.